

Supporting Information

Three Birds, One Stone – Photo-/Piezo-/Chemochromism in OneConjugated Nanoporous Ionic Organic Network

Jian-Ke Sun,⁺Ya-Jun Zhang,⁺ Gui-Peng Yu, Jie Zhang,^{*} Markus Antonietti, and Jiayin Yuan^{*}

1. Characterization methods.

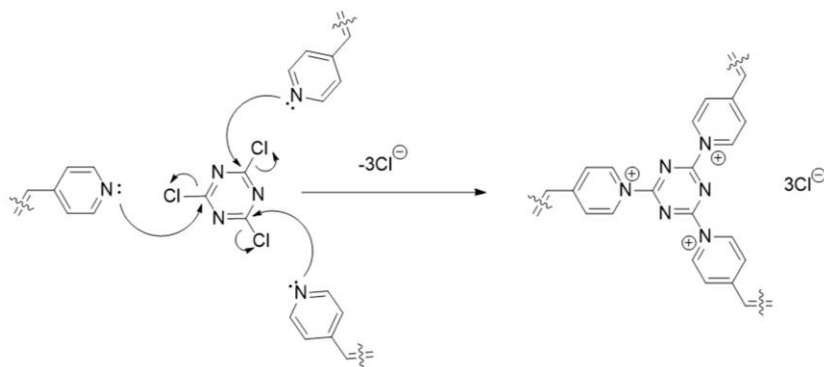
All chemicals were from commercial sources and used without further purification.

The morphology of the sample was visualized using a Gemini scanning electron microscope (SEM) under 3 kV (acceleration voltage). Energy-dispersive X-ray (EDX) mapping and analysis were taken on the SEM with an EDX spectrometer. N₂ sorption analysis was performed at 77 K on a QUADROSORB SI, equipped with automated surface area and pore size analyzer. Before analysis, samples were degassed at 100 °C for 12 h using a masterprep degassing system. Vapor-phase adsorption isotherms were measured with the Intelligent Gravimetric Sorption Analyser IGA100B of Hiden Corporation. Elemental analyses were done by the H. Kolbe MikroanalytischesLaboratorium. Powder X-ray diffraction (PXRD) patterns were recorded on a MiniFlexdiffractometer with Cu K α ($\lambda = 1.5406 \text{ \AA}$) at a scan speed of 4° min^{-1} with a glass holder. Thermal gravimetric analysis (TGA) measurement was recorded on NETZSCH STA 449 C. X-ray photoelectron spectroscopy (XPS) studies were performed with a ThermoFisher ESCALAB250 X-ray photoelectron spectrometer (powered at 150 W) using Al K α radiation ($\lambda = 8.357 \text{ \AA}$). To compensate the surface charging effects, all XPS spectra were referenced to the C 1s neutral carbon peak at 284.6 eV. The photochromic reaction was induced by irradiation with a Xe lamp (Beijing, 500 W). The solid UV-Vis diffuse reflectance spectra were recorded using a Lambda 950 spectrophotometer with BaSO₄ as a reference. The solution UV-Vis absorption measurements were recorded on a Lambda

900 spectrophotometer. Electron spin resonance (ESR) signals were determined by a BrukerA300 EPR spectrometer. Solid-state ^{13}C nuclear magnetic resonance (^{13}C -NMR) measurements were carried out at room temperature on a Bruker-BioSpinAVANCE III HD spectrometer. Fourier transform infrared spectroscopy studies (FT-IR) were recorded on a Bomem MB-102 FT-IR spectrometer. Raman spectra were recorded on a Labram HR Evolution spectrometer made by Horiba JobinYvon Corporation with laser wavelength of 532 nm.

2. Synthesis of NION-Cl. Cyanuric chloride (1.138g, 6.2mmol) was dissolved in 30 mL ethyl acetate and then dropwise added into a stirred solution of 1,2-bis(4-pyridyl)ethylene (1.638 g, 9 mmol) in 50 mL ethyl acetate, and the temperature remained 100°C for 48 h. The precipitate was obtained by filtration and washed with ethyl acetate for three times, then it was dried in a vacuum, giving the product as light brown powder (yield: $>90\%$).

The reaction is made by aromatic nucleophilic substitution on cyanuric chloride with the 1,2-bis(4-pyridyl)ethylene (Scheme S1). Similar type of reactions has been reported in previous literatures.¹⁻⁴ The nucleophilic character of the 1,2-bis(4-pyridyl)ethylene is comparable to standard pyridines bearing identical substituents.^{1a}



Scheme S1. A proposed reaction mechanism of nucleophilic substitution for the synthesis of NION-Cl.

Silver chloride quantitative analysis was performed by treating a certain amount of the dry sample in water with concentrated HNO_3 , followed by filtration of the supernatant liquid. The silver nitrate solution was added into above solution to give a white precipitate, which was

further isolated and washed with water and acetone and dried at 80°C prior to its weighting. The silver chloride quantitative analysis revealed an anion exchange capability is nearly half (48 %) of theoretical expected (7.2 mmol g⁻¹). Such discrepancy suggested that a half of the chloride counterions are consumed in the reduction of the bipyridinium rings thus leaving a partially radical state. Moreover, the Cl elemental analysis found for dry sample Cl: 17.76% agree well within the calculate one (Cl: 16.97 %) from the expected network, if only a half of Cl⁻ anion left in the network.

Reference:

- [1] S. Brasselet, F. Cherioux, P. Audebert and J. Zyss, *Chem. Mater.*, **1999**, 11, 1915-1920.
- [2] F. Cherioux and P. Audebert, *Chem. Mater.*, **1998**, 10, 1984-1989.
- [3] A. B. Bourlinos, P. Dallas, Y. Sanakis, D. Stamopoulos, C. Trapalis and D. Niarchos, *Eur. Polym. J.*, **2006**, 42, 2940-2948.
- [4] A. Schmidt and A. Hetzheim, *Tetrahedron*, **1997**, 53, 1295-1300.

3. Additional Figures and Data.

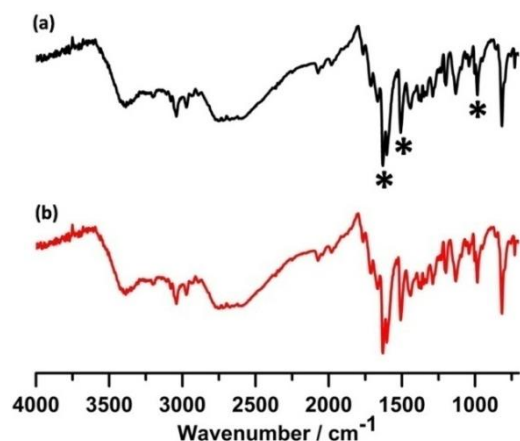


Figure S1. The FT-IR spectra of NION-Cl before and after photoirradiation. The bands labeled by asterisks at 980 and 1500 cm^{-1} are ascribed to the vibration of the olefin bond and the triazine ring, respectively. The band labeled by asterisks at 1630 cm^{-1} is attributed to the characteristic for the generated pyridinium cation. The strong C-Cl stretching vibration band of cyanuric chloride at 850 cm^{-1} vanished after the reaction, suggesting a quantitative replacement of Cl atoms on the triazine ring by 4,4'-bpe. The bands at 984 and 1508 cm^{-1} ascribed to the vibration of the olefin bond in 4,4'-bpe and the triazine ring, respectively, appear in the spectrum of NION-Cl as their addition product. Meanwhile, an intense band at 1630 cm^{-1} characteristic for pyridinium cations is found in NION-Cl, supporting a larger extent of the substitution reaction.

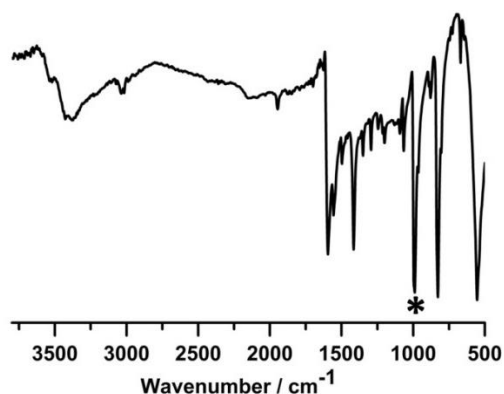


Figure S2. The FT-IR spectra of 4,4'-bpe. The band labeled by asterisks at 989 cm^{-1} is attributed to the characteristic C-H vibration of *trans* olefin unit.

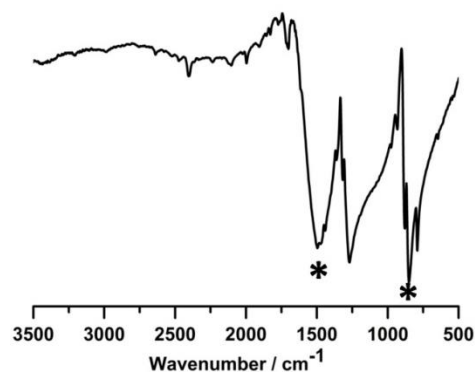


Figure S3. The FT-IR spectra of 2,4,6-trichloro-1,3,5-triazine. The bands labeled by asterisks at 1496 and 850 cm^{-1} are attributed to the characteristic C=N and C-Cl vibration of triazine ring, respectively.

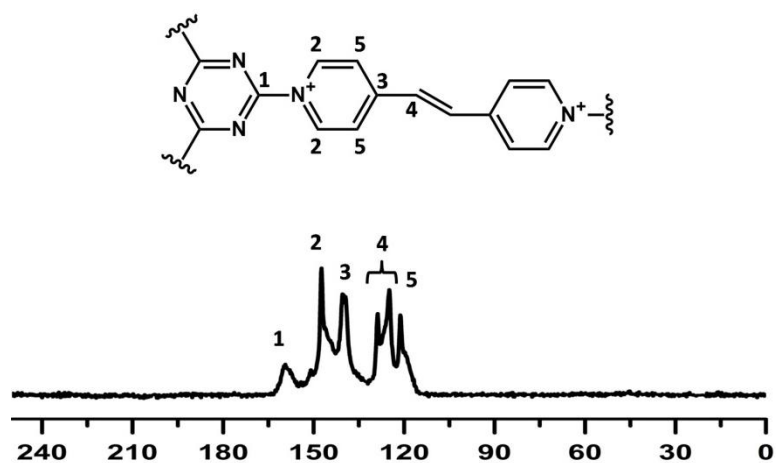


Figure S4. The solid-state¹³C-NMR spectra of NION-Cl, the corresponding carbon atoms are labeled.

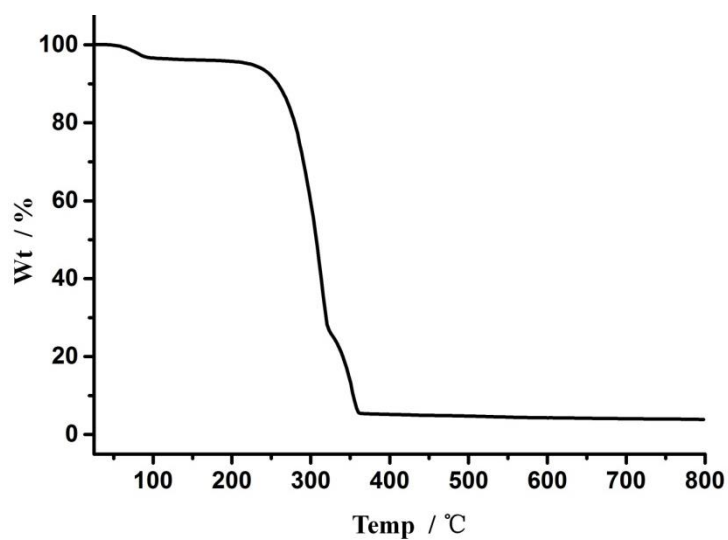


Figure S5. TGA curve of NION-Cl. The weight loss before 90 °C is attributed to the removal of absorbed solvent in NION-Cl.

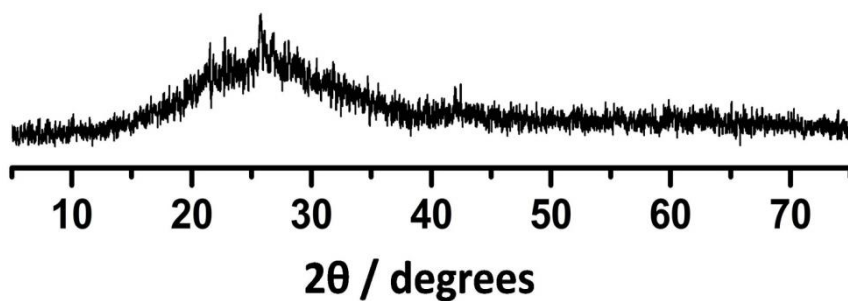


Figure S6. The PXRD pattern of NION-Cl.

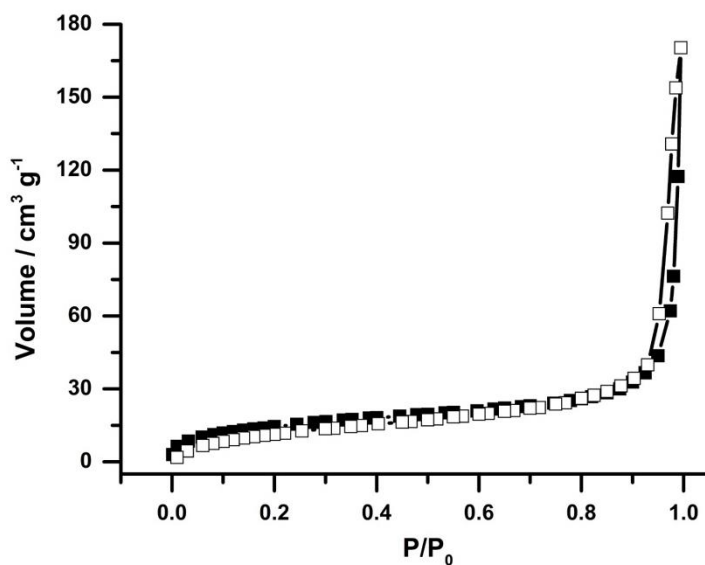


Figure S7. The nitrogen sorption isotherms of NION-Cl at 77 K.

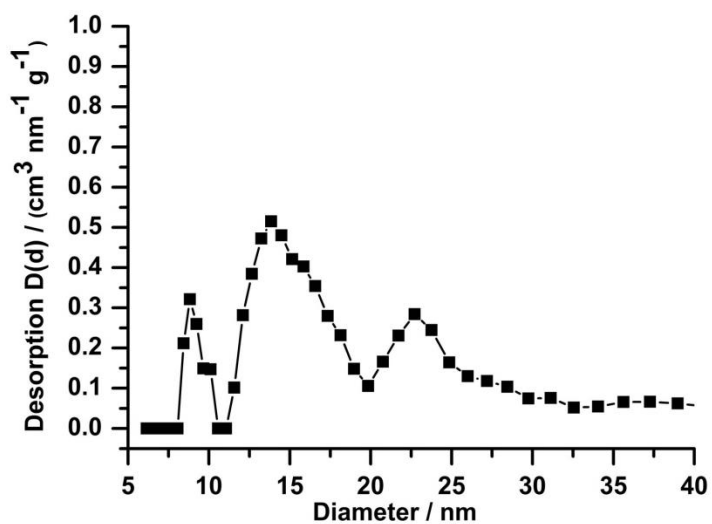


Figure S8. The pore size distributions of NION-Cl determined by density function theory.

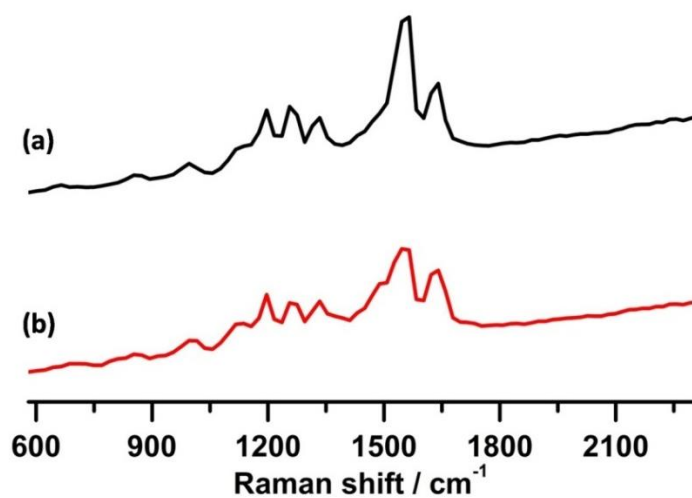


Figure S9. The Raman spectra of NION-Cl before (a) and after (b) Xe lamp irradiation.

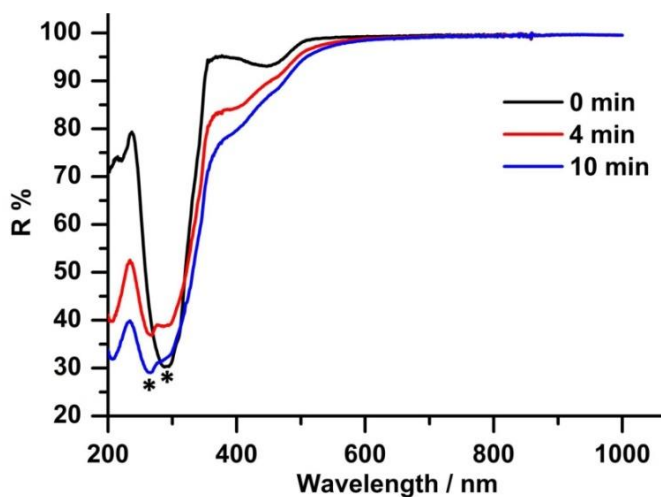


Figure S10. The time-dependent UV-Vis diffuse reflectance spectra of 4,4'-bpe monomer upon continuous photoirradiation. An increasing absorption band at 255 nm (labeled by asterisk) with concurrently decreasing another band at 300 nm (labeled by asterisk) after irradiation was observed.

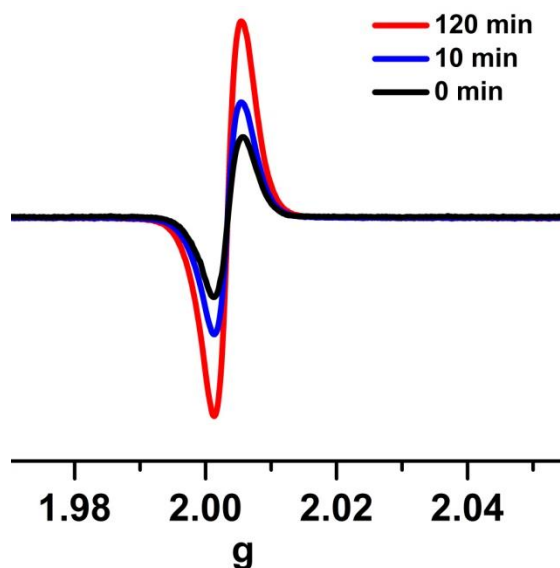


Figure S11. The time-dependent ESR signal generated by continuous photoirradiation.

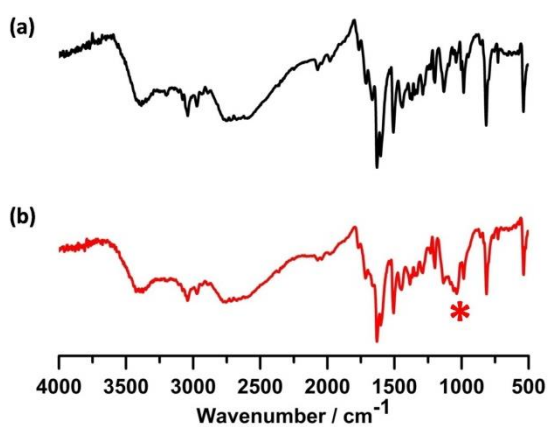


Figure S12. The FI-IR spectra of NION-Cl before (a) and after (b) exchange with BF_4^- anion, the characteristic of BF_4^- represented with the red asterisk.

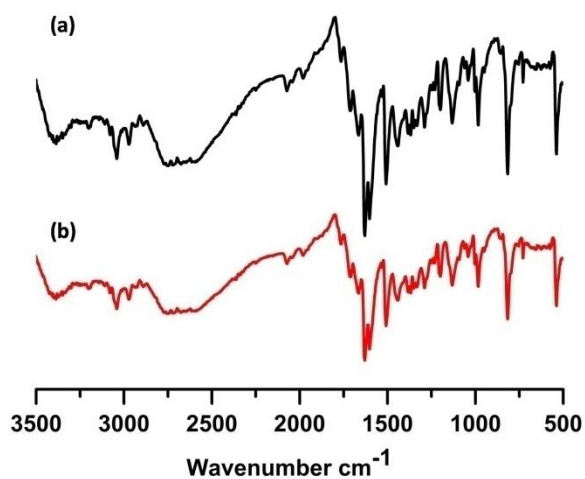


Figure S13. The FT-IR spectra of NION-Cl before (a) and after (b) piezochromism.

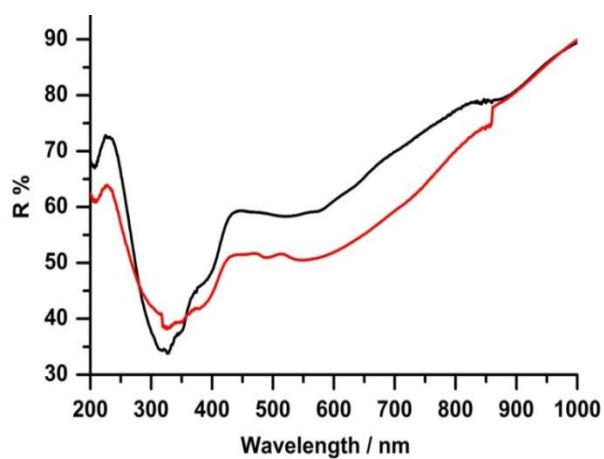


Figure S14. The UV-Vis diffuse reflectance spectra before (black) and after (red) piezochromism.

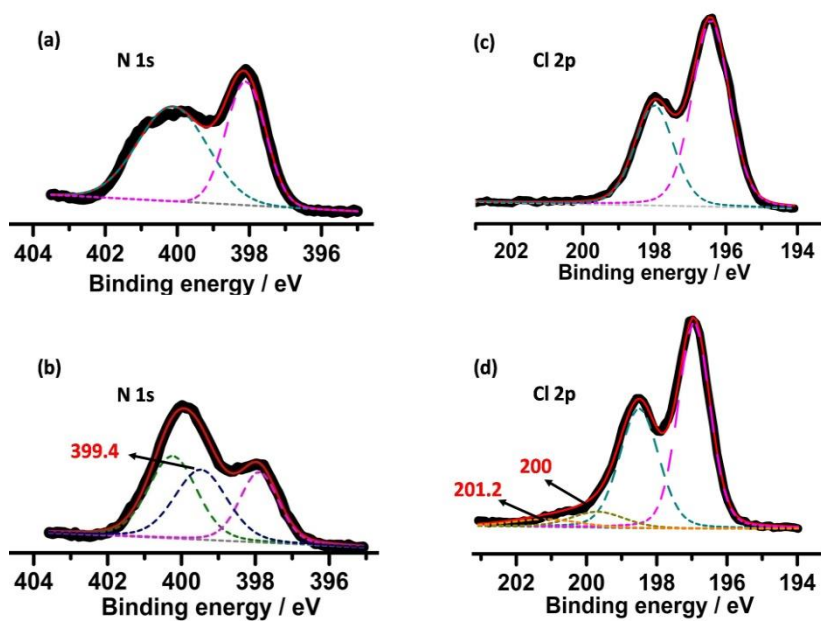


Figure S15. XPS core-level spectra of N 1s and Cl 2p before (a, c) and after (b, d) piezochromism. The dashed lines depict the resolved peaks. The sum of which is shown by red solid line. The original N 1s core-level spectrum can be fitted to two peaks at 400.2 and 398.1 eV, attributed to the N atoms of pyridine/pyridinium and triazine ring, respectively (a). After piezochromism, a new peak emerged at a position of a lower binding energy (399.4 eV) in addition to pyridinium N 1s (b), indicating that a part of pyridinium nitrogens are reduced and moved to the lower electron binding energy. As for Cl 2p after piezochromism, beside the negatively charged Cl (Cl 3d_{5/2} and 3d_{3/2} at 196.6 and 198.6 eV, respectively), other two new peaks lying at 200 and 201.2 eV appeared that could be attributed to partial generation of neutral Cl atom, suggesting that Cl⁻ anion lost electrons. Such evidence reveals that ET process should arise from electron rich Cl⁻ anion to electron deficient N⁺ cation in pyridinium ring.

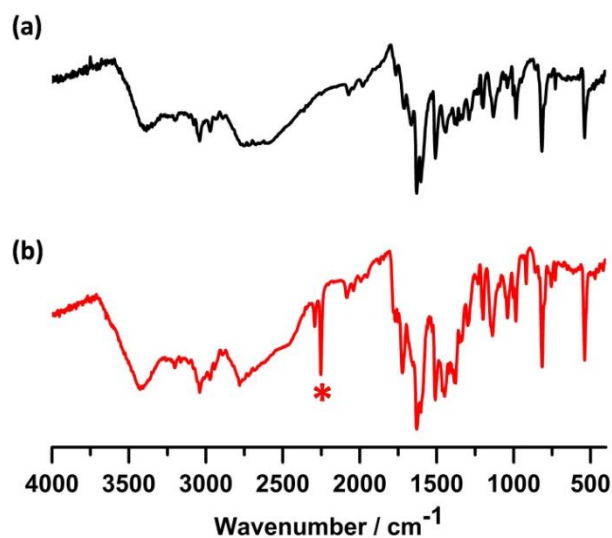


Figure S16. The FI-IR spectra of NION-Cl before (a) and after (b) immersing in CH₃CN, the characteristic of CH₃CN represented with the red asterisk, and the incorporated CH₃CN can be totally removed to achieve initial state (a) under vacuum condition via thermal-treatment.

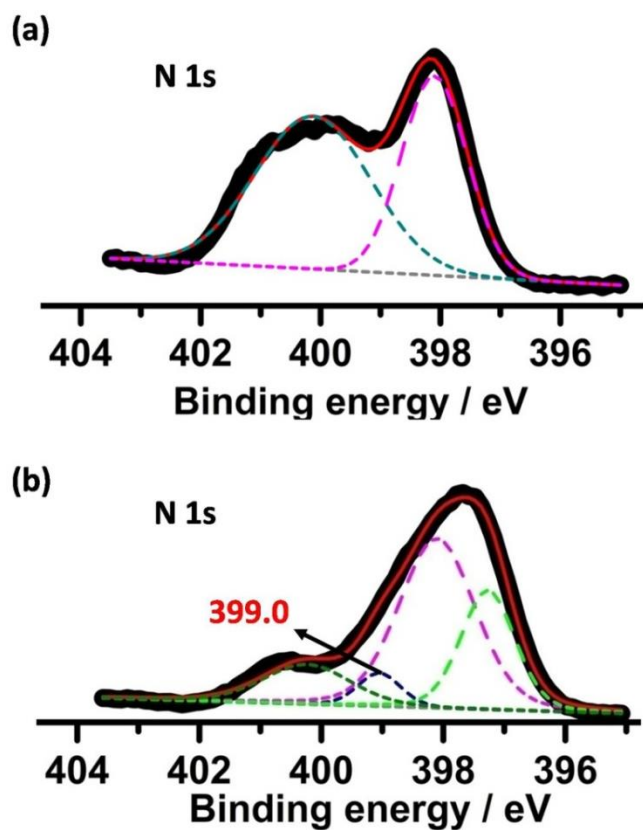


Figure S17. XPS core-level spectra of N 1s before (a) and after (b) solvochromism. The dashed lines depict the resolved peaks, the sum of which is shown by red solid line. The original N 1s core-level spectrum can be fitted to two peaks at 400.2 and 398.1 eV, attributed to the N atoms of pyridine/pyridinium and triazine ring, respectively (a). After solvochromism, the N 1s core-level spectrum can be fitted to four peaks (b). In addition to the peaks at 400.2, 398.1 and 397.3 eV that were attributed to the N atoms of pyridine/pyridinium, triazine ring and CH_3CN , respectively, a new peak emerged at a position of a lower binding energy (399.0 eV) in addition to pyridinium N 1s, indicating that a part of pyridinium nitrogens are reduced and moved to the lower electron binding energy.

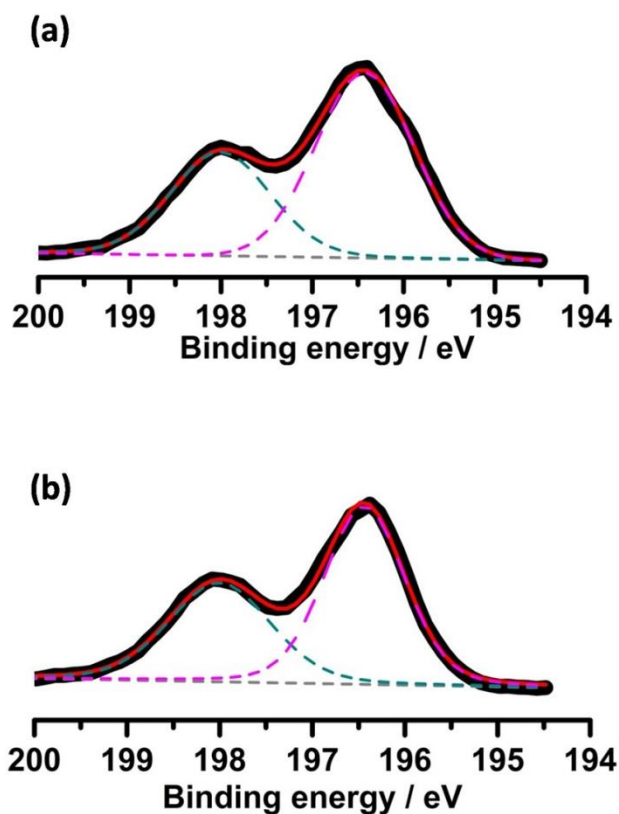


Figure S18. XPS core-level spectra of Cl 2p before (a) and after (b) solvochromism. The dashed lines depict the resolved peaks, the sum of which is shown by red solid line. No detectable shift of Cl 2p core could be observed in the solvochromism process, indicating the Cl⁻ does not involve in the electron transfer process.

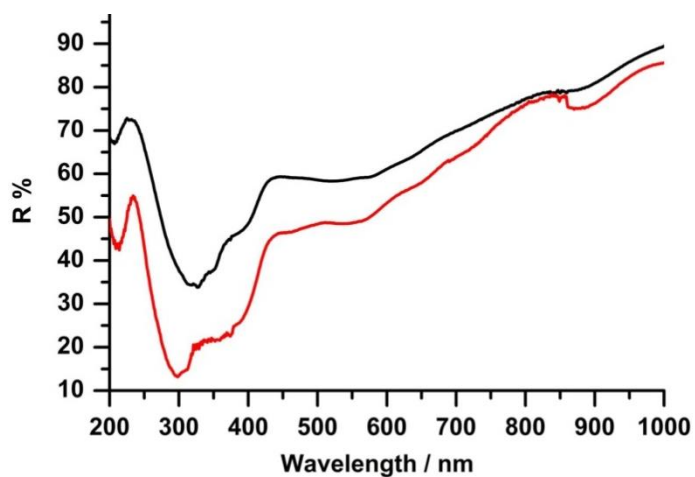


Figure S19. The UV-Vis diffuse reflectance spectra before (black) and after (red) solvochromism.

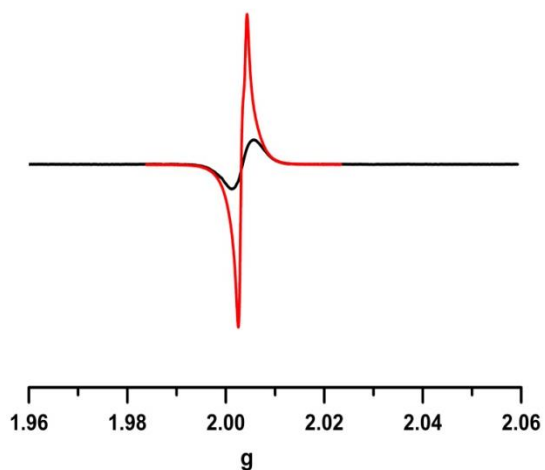


Figure S20. The ESR signal before (black) and after (red) solvochromism of NION-Cl.

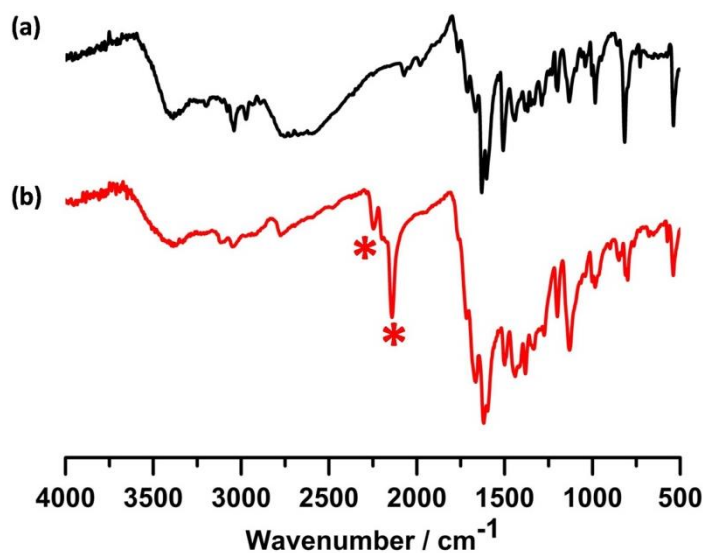


Figure S21. The FI-IR spectra of NION-Cl before (a) and after (b) immersing in $\text{N}(\text{CN})_2^-$ containing solution. The sample b was then washed several times with pure ethanol. The characteristic band for $\text{N}(\text{CN})_2^-$ is labeled with a red asterisk, indicating the anion was chemically incorporated into the pore.

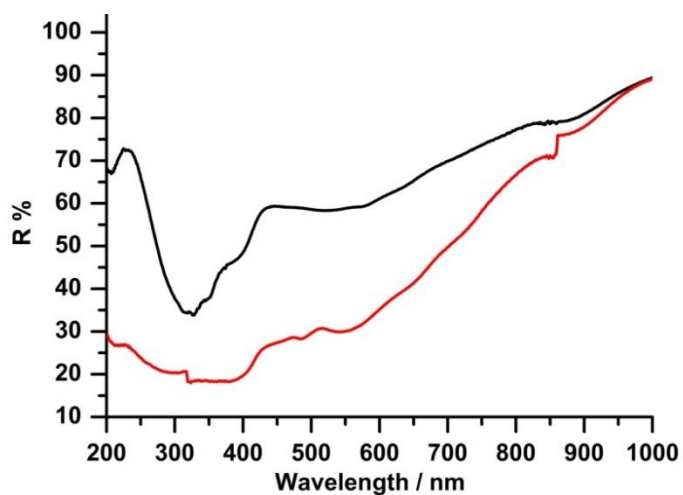


Figure S22. The UV-Vis diffuse reflectance spectra of NION-Cl before (black) and after (red) anionochromism. The enhanced absorbance in the visible light range explained the darkened color of the sample.

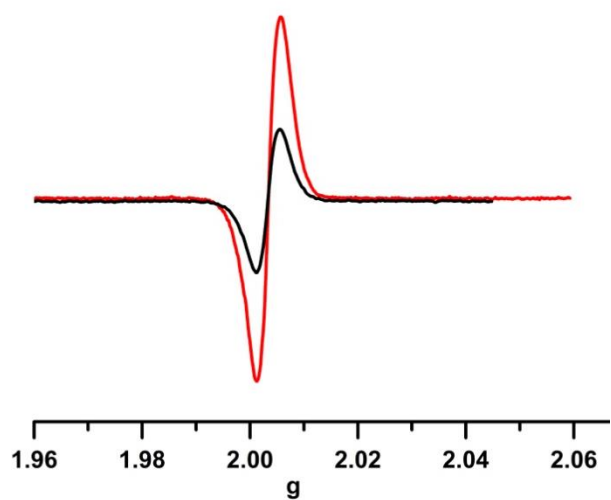


Figure S23. The ESR signal of NION-Cl before (black) and after (red) anionochromism. The enhanced radical signal indicated the appearance of more radicals upon treatment with $\text{N}(\text{CN})_2^-$ anions.

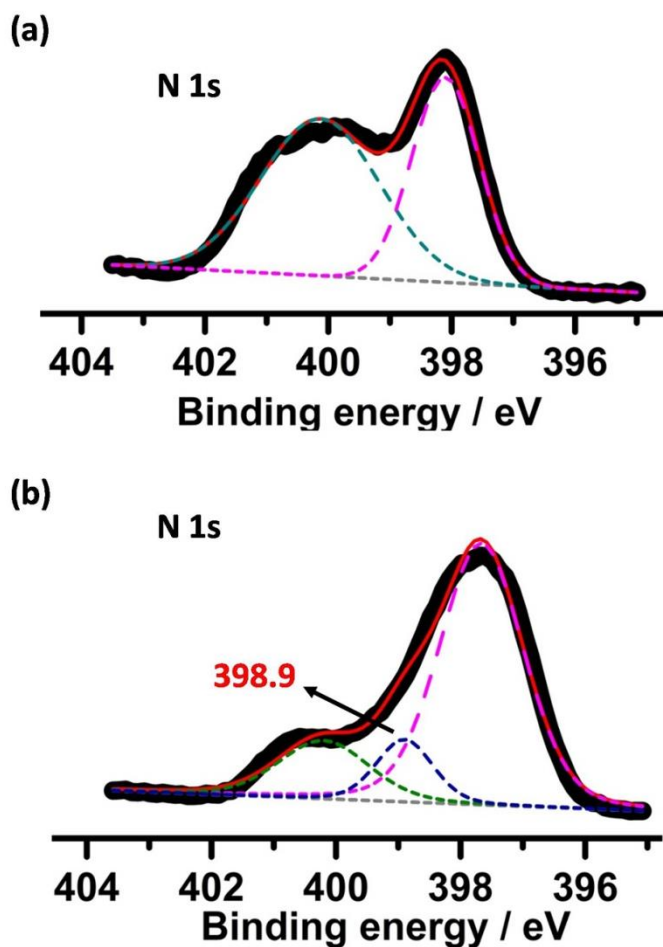


Figure S24. XPS core-level spectra of N 1s before (a) and after (b) anionochromism. The dashed lines depict the resolved peaks. The sum of which is shown by red solid line. The original N 1s core-level spectrum can be fitted to two peaks at 400.2 and 398.1 eV, attributed to the N atoms of pyridine/pyridinium and triazine ring, respectively (a). Due to complicated N species in $\text{N}(\text{CN})_2^-$, the N 1s core-level spectrum after anionochromism was fitted to three peaks. The peaks at 400.2 and 397.7 eV were attributed to the N atoms of pyridine/pyridinium, sum of triazine ring and $\text{N}(\text{CN})_2^-$ anion, respectively. The new peak emerged at a position of 398.9 eV with a lower binding energy (400.2 eV) is attributed to a part of pyridinium N atom shift after receiving electrons.

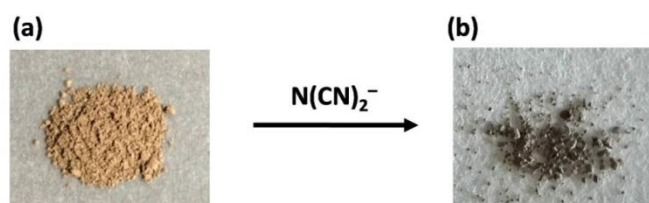


Figure S25. The image of NION-Cl before (a) and after (b) treatment with $\text{N}(\text{CN})_2^-$ containing solution (10 ppm).

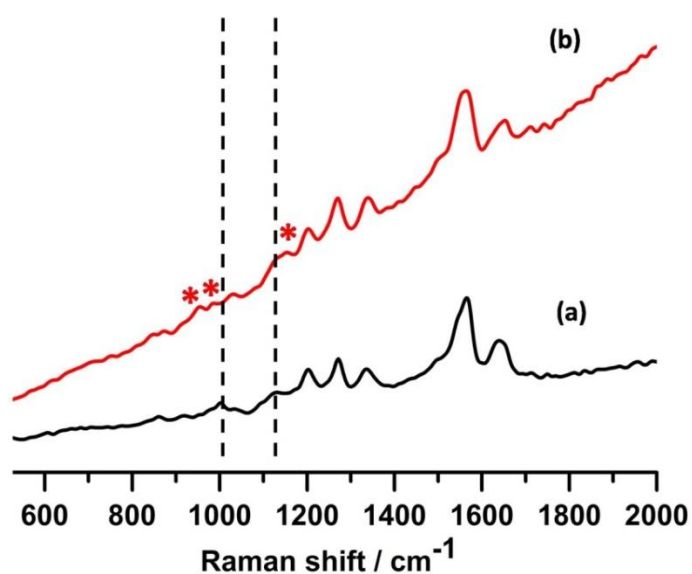


Figure S26. Raman spectra of NION-Cl before (a) and after (b) vapochromism. From the spectra we can see that the pyridinium ring breathing peak at 1000 cm^{-1} disappears with the emergence of new peaks at 985 and 952 cm^{-1} . Another obvious change is the stretching mode of C–C bond (1129 cm^{-1}) in the pyridinium that also shifted by ammonia fumigation. These observations are consistent with previous evidence in literature (C. Chen, L. X. Cai, B. Tan, Y. J. Zhang, X. D. Yang and J. Zhang, *Chem. Commun.* 2015, 51, 8189).

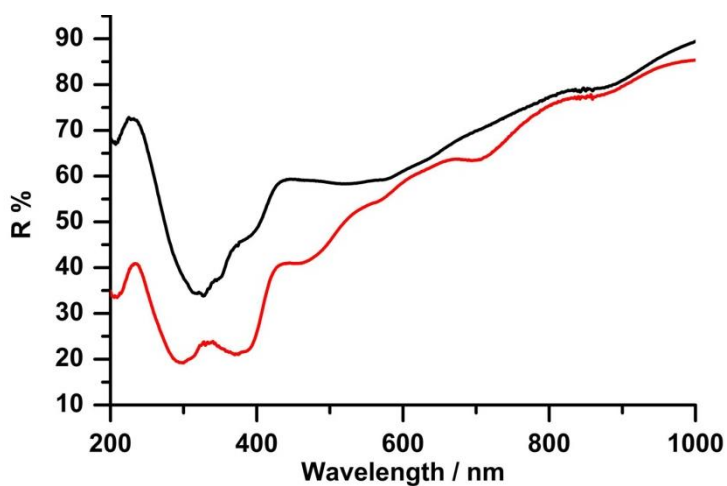


Figure S27. The UV-Vis diffuse reflectance spectra of NION-Cl before (black) and after (red) vapochromism.

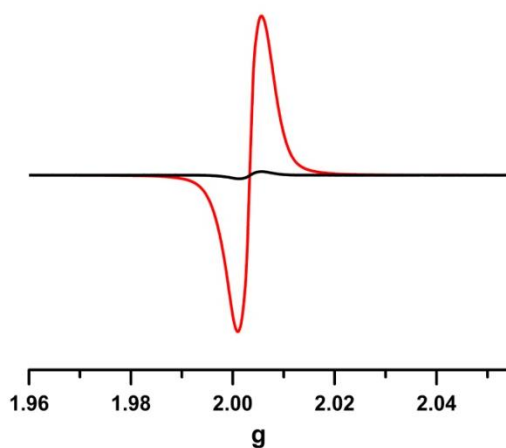


Figure S28. The ESR signal of NION-Cl before (black) and after (red) vapochromism.

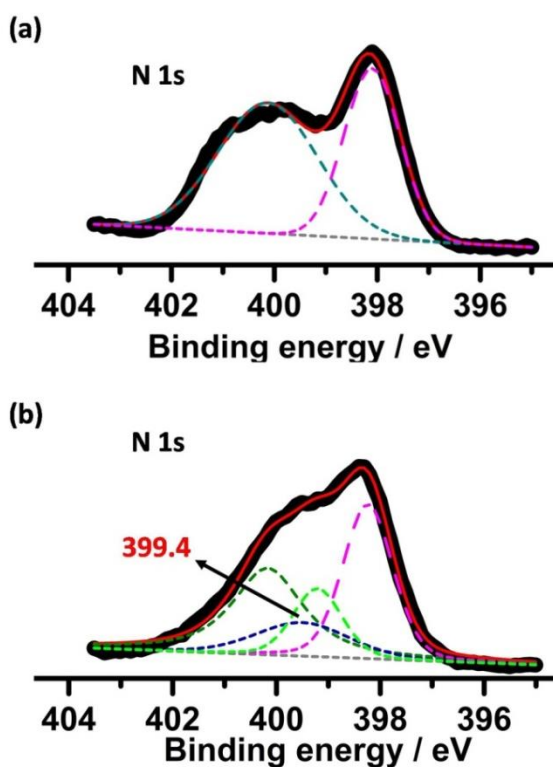


Figure S29. XPS core-level spectra of N 1s before (a) and after (b) vapochromism. The dashed lines depict the resolved peaks, the sum of which is shown by red solid line. The original N 1s core-level spectrum can be fitted to two peaks at 400.2 and 398.1 eV, attributed to the N atoms of pyridine/pyridinium and triazine ring, respectively (a). After vapochromism, the N 1s core-level spectrum can be fitted to four peaks (b). In addition to the peaks at 400.2, 399.2 and 398.1 eV, attributed to the N atoms of pyridine/pyridinium, NH_3 , and triazine ring, respectively, a new peak emerged at a position of a lower binding energy (399.4 eV) in addition to pyridinium N 1s (400.2 eV), indicating that a part of pyridinium nitrogens are reduced and moved to the lower electron binding energy.